Effects of fermion flavor on exciton condensation in double-layer systems

J. Shumway[1] and Matthew J. Gilbert[2,3,*]

[1]*Department of Physics, Arizona State University, Tempe, Arizona 85287, USA*

[2]*Department of Electrical and Computer Engineering, University of Illinois, Urbana, Illinois 61801, USA*

[3]*Micro and Nano Technology Laboratory, University of Illinois at Urbana-Champaign, Urbana, Illinois 61801, USA*

(Received 23 December 2011; published 23 January 2012)

We use a fermionic path-integral quantum Monte Carlo framework to study the effects of fermion flavor on the physical properties of dipolar exciton condensates in double-layer systems. We find that by including spin in the system the effective interlayer interaction strength is weakened, yet this has very little effect on the Kosterlitz-Thouless transition temperature. We further find that, to obtain the correct description of screening, it is necessary to account for correlation in both the interlayer and intralayer interactions. We show that while the excitonic binding cannot completely suppress screening by additional fermion flavors, their screening effectiveness is reduced by intralayer correlations leading to much higher transition temperatures than predicted with large-N analysis.

DOI: 10.1103/PhysRevB.85.033103 PACS number(s): 71.35.Lk, 73.63.−b, 71.10.−w

Dipolar fermionic condensates have been a topic of great interest in a diverse assortment of physical systems for many years. Recently, double-layer systems—two spatially segregated quantum systems—have provided a fruitful playground in which to study dipolar superfluidity in microcavities,[1,2] cold-atom systems,[3–7] and semiconductor quantum wells.[8–13] Interest in dipolar superfluids has received increased attention due in large part to the prediction of dipolar superfluid behavior at or above room temperature in double-layer graphene.[14–16] This is uniquely possible in graphene due to the symmetric linear band structure and ability to sustain large carrier concentrations in two closely spaced layers. Yet, this prediction is not without significant controversy. As superfluidity is predicted to occur in the double-layer graphene system outside of the quantum Hall regime, additional fermion flavors, or degrees of freedom, beyond the top- or bottom-layer freedom may participate in the phase transition. Theoretical disagreements over the Kosterlitz-Thouless transition temperature (T_{KT}) arise from differing assumptions about the importance of these extra flavors for screening in dipolar exciton condensates. In the works predicting a high transition temperature of $T_{\mathrm{KT}} \approx 0.1\ T_{\mathrm{F}}$ (where T_{F} is the system Fermi temperature) the fermionic degrees of freedom in the system were taken to be constrained by the large energy gap formed when the interacting electrons and holes bind. The quasiparticles lose their individual fermionic character and cannot screen interlayer interactions, which does not result in a significantly lower T_{KT}. Other works on the same double-layer graphene system predict a low transition temperature of $T_{\mathrm{KT}} \approx 10^{-7}\ T_{\mathrm{F}}$ by assuming that screening from additional degrees of freedom add independently to effectively screen out the interlayer interaction.[17,18] This assumption leads to the conclusion that screening in condensate is as strong as in the normal phase and results in the small value for T_{F}. While experiment will be the ultimate arbiter of the value of T_{KT}, many-body theoretical approaches will play a significant role in understanding the nature of the phase transition. Recent experiments in double-layer graphene[19] have shown tantalizing signs of interlayer coherence but no signs of a dipolar exciton condensate which would manifest itself through a number of observables such as the presence of an interlayer critical current.[12,20]

In this Brief Report, we use a fermionic path-integral quantum Monte Carlo (PIMC)[21,22] framework to elucidate the role of screening in exciton condensates formed in symmetric electron-hole double-layer systems. We show that increased fermion flavor does increase the screening in exciton condensates formed in a symmetric double-layer system. However, the role of screening is not as dramatic as predicted in existing analytic work, because of both strong excitonic pairing and the presence of intralayer correlations not previously considered. We compare the static correlations and dynamic response functions of symmetric electron-hole double-layer systems with different numbers of fermionic flavors. We show that, when the spin degree of freedom is included in our simulations, the transition temperature for our system drops roughly with T_{F}. Additionally, we use a dynamic density-density response function, collected within the PIMC framework, to demonstrate that, when the spin degree of freedom is included, the polarizability of the system actually decreases. This decrease corresponds to a complicated interplay between Pauli exclusion forcing identical carriers in the same layer to avoid one another and the fact that neutral excitons do not screen charge effectively.

We use a symmetric model for electrons and holes in two parallel, two-dimensional sheets, separated by a $d = 0.5$ nm SiO_2 tunnel barrier with a relative dielectric constant of $\epsilon_r = 3.9$. The Hamiltonian for our system includes the kinetic energy of the quasiparticles and Coulomb interactions:

$$H = \sum_{i=1}^{N_e} \frac{p_{i,e}^2}{2m^*} + \sum_{i=1}^{N_h} \frac{p_{i,h}^2}{2m^*} + \sum_{i<j} \frac{e^2}{\epsilon |\mathbf{r}_{i,e} - \mathbf{r}_{j,e}|} + \sum_{i<j} \frac{e^2}{\epsilon |\mathbf{r}_{i,h} - \mathbf{r}_{j,h}|} - \sum_{i,j} \frac{e^2}{\epsilon \sqrt{|\mathbf{r}_{i,h} - \mathbf{r}_{j,e}|^2 + d^2}}. \quad (1)$$

All quasiparticles have equal mass of $m = 0.09 m_e$, so that the Fermi velocity approximates the velocity of quasiparticle in graphene.[15] In this work we separately consider the cases of spinless and spin-1/2 quasiparticles, corresponding to different numbers of fermion flavors: $N_f = 2$ when the carriers only have a layer degree of freedom, and $N_f = 4$ when the carriers have both layer and spin degrees of freedom. Each

of the layers in our system is assumed to be 20 nm × 20 nm with periodic boundary conditions the plane of the layers. We use $N = 40$ quasiparticles in our simulations consisting of 20 electrons in the top layer and 20 holes in the bottom layer. The number of electrons and holes corresponds to carrier densities of $n_e = n_h = 5 \times 10^{12}$ cm^{-2} and places the system in the the regime where the exciton condensate has been predicted to exist.[14–16] When simulations with spin are performed, $N_f = 4$, we use 10 spin-up and 10 spin-down particles per layer. As the Hamiltonian does not have any spin-dependent terms, the spin only enters into the calculation when considering fermion antisymmetry upon particle exchange. The Coulomb interactions are handled within the pair approximation, and the path is discretized with a time step $\hbar\,\Delta\tau \approx 3$ Ha^{-1}. To circumvent the well-known fermion sign problem in our simulations, we use a ground-state fixed-node approximation,[23,24] as used in three-dimensional excitonic Bose-Einstein condensate (BEC) studies.[25] At each imaginary time slice, we require that the electron and hole coordinates lead to a positive Slater determinant, $\det|\phi(r_{e,i} - r_{h,j})|$, where $\phi = e^{-r/a}$ is the typical BCS mean-field pairing wave function typically used in quantum Monte Carlo simulations of exciton condensation in symmetric electron-hole systems.[26,27] For our simulations, we have used an exciton pairing radius a of 2.3 nm but have performed simulations containing $a = 1$–10 nm and find our results to be insensitive to this parameter.

In Fig. 1(a), we show our calculated superfluid fraction as a function of the system temperature. Our calculations reveal a suppressed T_{KT} when the additional spin degree of freedom is included. Superfluid fraction is an excellent way to understand

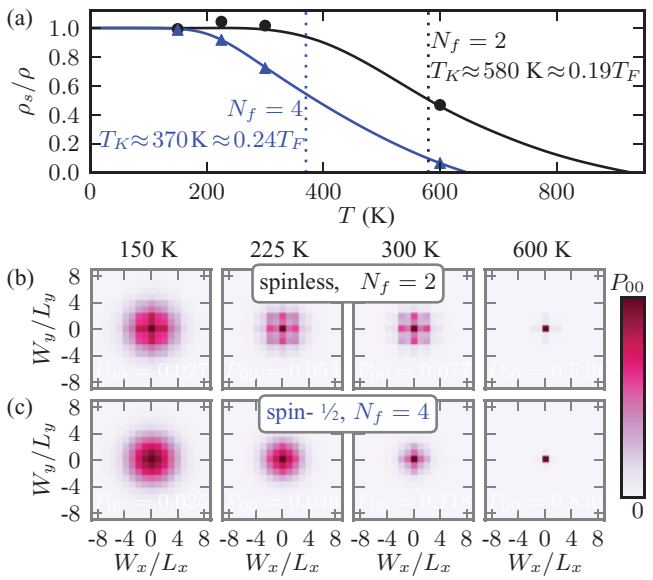

FIG. 1. (Color online) (a) Superfluid fraction for spinless (black circles, $N_f = 2$) and spin-1/2 (blue triangles, $N_f = 4$) symmetric double-layer electron-hole condensate, calculated from PIMC simulations of 40 electron-hole pairs. Estimates of T_{KT} are made where the superfluid fraction drops to 1/2, and lines are a guide to the eye. We plot normalized histograms of topological winding distributions, which measure superfluid density, Eq. (2), for the (b) spinless and (c) spin-1/2 cases. P_{00} represents the probability height of the (0,0) point in the histograms.

phase transitions in systems as it saturates at 1 for low temperatures and asymptotes to 0 beyond the phase boundary. We denote the T_{KT} as the temperature where the superfluid fraction has dropped to 0.5 to be consistent with previous work.[28] We see a clear drop in T_{KT} from $T_{\mathrm{KT}} \approx 580$ K in the spinless case to $T_{\mathrm{KT}} \approx 300$ K in the spin-1/2 case, illustrating the effect of increased fermion flavor on the phase transition. In fact, this drop in transition temperature may be understood without resorting to screening arguments. One would expect a decrease in T_{KT} simply from reduced quantum degeneracy as more fermion flavors are added. In an ideal Bose gas, the magnitude of the transition temperature is determined by the condition $n\lambda(T_{\mathrm{KT}})^2 \sim 1$, where $\lambda(T) \sim T^{-1/2}$ is the thermal de Broglie wavelength and n is the density of identical bosons. As fermions pair into bosons, there must be at least N_f distinguishable species of bosons, decreasing the density, n, and hence, the transition temperature T_{KT} by $1/N_f$. This effect of reduced quantum degeneracy can also be seen by comparing T_{KT} to the Fermi temperature which, at our density, corresponds to $T_{\mathrm{KT}}^{\mathrm{sp}} \approx 0.19 T_{\mathrm{F}}$ to $T_{\mathrm{KT}}^{\mathrm{sp}} \approx 0.24 T_{\mathrm{F}}$ showing that T_{KT} scales closely with T_{F}. This indicates the increased number of fermion flavors in our system are not completely screened by the condensate.

Path integrals allow for the calculation of a variety of properties of the condensate and the phase transition to help explain the decrease in T_{KT}. In the path integral, particle statistics enter through permutations: particles' paths may end on neighboring identical particles. The superfluid transition is seen as percolation because below T_{KT} paths of particles span the solution domain. The calculated superfluid fraction is estimated by the presence of permuting paths that wind around the periodic box.[22] In two dimensions, the superfluid fraction is given by

$$\frac{\rho_s}{\rho} = \frac{mk_B T}{\hbar^2 (N_e + N_h)} \langle W_x^2 + W_y^2 \rangle. \qquad (2)$$

In Eq. (2), W_x and W_y are the topological windings (which are integer multiples of the supercell dimensions) corresponding to the different path configurations. For excitonic condensates, we use the number-coupled winding, where W_x and W_y each include a sum over individual windings of electron and hole quasiparticles. When electrons and holes are tightly paired in excitons, even windings dominate the histogram since a winding electron must be accompanied by a winding hole. Were the electrons and holes simply correlated and not condensed, then there would be no winding about the simulation region and we would only see the trivial peak at $W_x = W_y = 0$. Therefore, looking at the histogram of the winding distributions can easily identify an excitonic condensate.

Figures 2(b) and 2(c) compare the exciton winding probabilities for the (a) spinless case and (b) spin-1/2 case for several temperatures. At $T = 150$ K, we see similar behavior for both systems, as each system is nearly all superfluid. The effect is more washed out in the spin-1/2 state, which we attribute to the relatively small number, ten, of identical fermions. Furthermore, we notice that the even peaks are accompanied by odd peaks in the winding, which are artifacts of the finite size simulations and the low system temperatures. Larger simulations should sharpen this even winding number signature of an excitonic condensate and eliminate the odd winding peaks. As we increase the system temperature, we again see peaks in the even

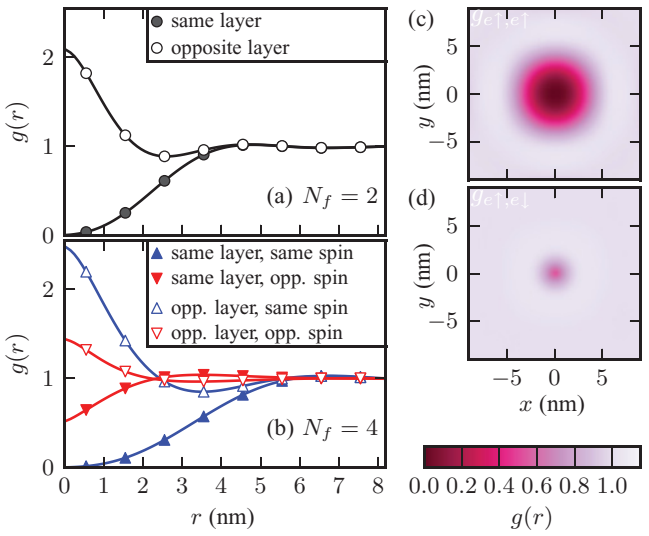

FIG. 2. (Color online) Radial pair correlation functions for (a) spinless, $N_f = 2$, and (b) spin-1/2, $N_f = 4$ cases. (c) Intralayer exchange-correlation hole for the same spin species, $g^{\uparrow\uparrow}(\mathbf{r}_{ij})$. (d) Intralayer correlation hole for opposite spin species, $g^{\uparrow\downarrow}(\mathbf{r}_{ij})$.

winding numbers at $T = 225$ K but we see a major difference at $T = 300$ K. We expect that the $N_f = 2$ system is still condensed but the $N_f = 4$ system is close to the phase boundary. We see weak even peaks in the $N_f = 4$ case but well-formed even peaks in the $N_f = 2$ case, showing the reduced superfluid fraction at this temperature with increased fermion flavor. At $T = 600$ K, we see only the trivial winding peak in $N_f = 4$ and some weak peaks in the $N_f = 2$ case corresponding to a temperature where both systems have passed the phase boundary.

To better understand the role of fermion flavors in the decrease in T_{KT}, we examine real-space static correlation among the quasiparticles due to Coulomb interactions and Pauli exclusion. We have collected the pair-correlation functions $g(r)$ by binning the equal-time pair distributions in a histogram. In contrast to other quantum Monte Carlo (QMC) methods, such as variational or diffusion Monte Carlo, there is no bias from a trial wave function; thus, PIMC gives essentially exact pair correlations, aside from errors associated with the fixed-node approximation. In Fig. 2 we show our calculated pair correlation functions at $T = 150$ K. We find the presence of an exchange hole in between identical fermions, which is larger in the $N_f = 4$ case simply because the density of particles of a particular flavor decreases as $1/N_f$. We find that there is a strong, attractive, interlayer correlation g^{eh}, with a peak at small separations that is coincident with the formation of indirectly bound excitons with holes in the top layer sitting directly above the electrons in the bottom layer. This pairing of identical spin states in the $N_f = 4$ case may be an artifact of our nodal model, where we have built or nodal wave function from a Slater determinant of orbitals pairing like spins only.

Interestingly, we find a small correlation hole for the $N_f = 4$ case, arising almost equally from the electron and hole of opposite spin: the particle in the same layer (with the same charge) is slightly repelled, while the particle in the opposite layer (with the opposite charge) is similarly attracted. This is a clear demonstration that extra fermion flavors correlate among one another, even when they do not bind as condensed excitons. This is more dramatically illustrated in Figs. 2(c) and 2(d). In Fig. 2, we plot the intralayer pair correlation in two dimensions corresponding to $g_{sp}^{\uparrow\uparrow}$ and, as expected, we see a large correlation hole where Pauli exclusion and Coulomb repulsion force other identical particles apart. However, when we include spin-1/2 particles and examine the intralayer correlation of $g_{sp}^{\uparrow\downarrow}$ in Fig. 2(c), we see a much weaker correlation hole.

Beyond the use of static correlation functions to understand the drop in T_{KT}, we explore the dynamic correlation functions, namely the polarizability. In Refs. 17 and 18, the large-N_f approximation strongly resembles the random phase approximation (RPA), and hence the screening they find is essentially the Lindhard function, with suppression of screening at very small q due a BCS-like excitonic condensate. In Fig. 3, we show that our calculated polarizabilities are considerably different. To collect the dynamic correlation functions we sample the polarization operator between different fermion flavors γ and γ',

$$\Pi_{\gamma\gamma'}(\mathbf{q}, i\omega_n) = -\frac{q_\gamma q_{\gamma'}}{V\hbar}\int_0^{\beta\hbar} \langle T_\tau\, n_{\mathbf{q},\gamma}(\tau) n_{-\mathbf{q},\gamma'}(0)\rangle\, d\tau, \quad (3)$$

where $n_{\mathbf{q},\gamma} = \sum_{i=1}^{N_\gamma} e^{i\mathbf{q}\cdot\hat{\mathbf{r}}_i}$ is the density operator for fermion flavor γ.

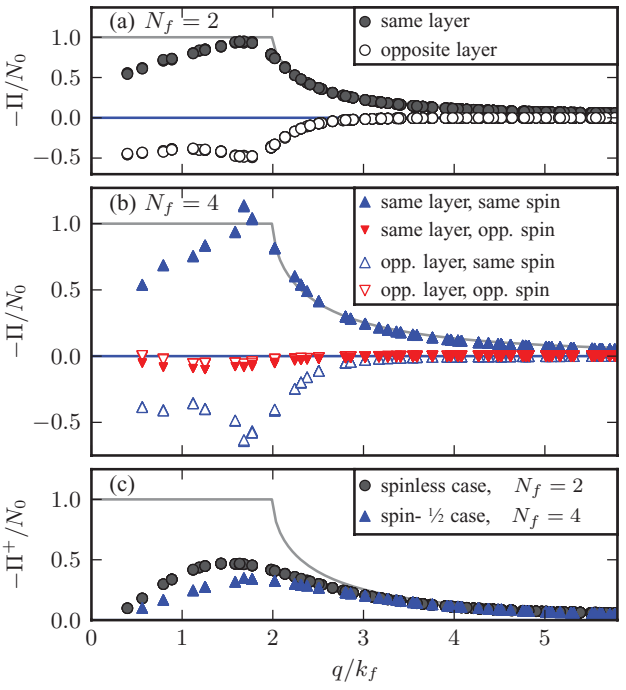

FIG. 3. (Color online) (a) Interlayer and intralayer polarizabilities for $N_f = 2$ vs the perturbation wave vector normalized by the Fermi wave vector. (b) Interlayer and intralayer polarizabilities for $N_f = 4$ normalized by the Fermi wave vector. (c) Sum of the interlayer and intralayer polarizabilities for $N_f = 2$ and $N_f = 4$ normalized by the Fermi wave vector. In each plot the polarizabilities are plotted against the Lindhard response function (shaded line) in two dimensions and have been normalized by the density of states at the Fermi energy in two dimensions, N_0.

In Fig. 3 we show the $\Pi_{\gamma,\gamma'}(\mathbf{q},0)$ between different fermion flavors normalized by the two-dimensional (2D) density of states as a function of wavelength normalized by the Fermi wave vector at a system temperature of $T = 150$ K. Here we find the polarization response from identical particles in $N_f = 2$ and $N_f = 4$ track the Lindhard function very well in the short wavelength limit, past $q > 2k_f$, as one would expect from Fermi liquid theory. Interestingly, we find similar behavior for both $N_f = 2$ and $N_f = 4$ in response to long wavelength excitations ($q \to 0$). This is expected as we are clearly in the condensate regime in which all carriers should be paired into excitons and, therefore, unable to respond to perturbations. The response between particles in different layers or of different spin is negative, indicating that these correlations suppress screening from the independent particle, corresponding to the RPA response. The response of the exciton is quite strong, denoted by the fact that the opposite-spin flavors have a weak negative response, Fig. 3(b). We have calculated the polarizabilities at temperatures both above and below T_{KT} and found very little difference between the different temperature traces for both the $N_f = 2$ and $N_f = 4$ cases, indicating that the screening behavior is dominated by preformed excitons, which exist above T_{KT}.

However, Fig. 3(c) shows that the sum of inter- and intralayer polarizabilities for $N_f = 4$ is smaller than that of $N_f = 2$. While the large-N calculation finds enhanced screening with increasing fermion flavors, N_f, we find a weaker trend. The reason for this difference is excitonic binding and correlation between different fermion flavors. In the large-N expansion, the starting point is RPA-like screening. Because each flavor can screen independently, the system exhibits weak BCS pairing of states near the Fermi surface when the temperature is below T_{KT}. In our simulations, we have strong excitonic pairing which organizes the quasiparticles into neutral excitons and suppresses their ability to screen. This excitonic pairing and correlation between quasiparticles of different spin is not present in the large-N approximation's perturbative expansion.

In conclusion, we have analyzed the static and dynamic response functions obtained from fermionic PIMC simulations of dipolar exciton condensates in symmetric electron-hole double-layer systems. We find that the addition of extra fermion flavors to the system reduces T_{KT} because the additional flavors are not screened out by the excitons in the condensate, thereby weakening the interlayer interaction strength which drives the transition from Fermi liquid to exciton condensate. Our analysis of polarizability shows that the strong excitonic pairing in our model suppresses screening, allowing a higher transition temperature. We find that while fermion flavors cannot be ignored, the drop in T_{KT} is not as large as predicted by the large-N expansion calculations because the system is in the strong-coupling regime and interlayer correlations are crucial to understanding the nature and temperature of the phase transition.

We wish to acknowledge M. Y. Alaoui Lamrani and Z. Estrada for help running the simulations. MJG is supported by the Army Research Office (ARO) under Contrat No. W911NF-09-1-0347. JS is supported by the Nanoelectronics Research Initiative (NRI) South West Academy of Nanoelectronics (SWAN). Computer simulations used the National Science Foundation TeraGrid and the ASU Advance Computing Center (A2C2).

*matthewg@illinois.edu

[1] R. B. Balili, V. Hartwell, D. Snoke, L. Pfeiffer, and K. West, Science **316**, 1007 (2007).
[2] S. Christopoulos, G. Baldassarri Hörger von Högersthal, A. Grundy, P. G. Lagoudakis, A. V. Kavokin, J. J. Baumberg, G. Christmann, R. Butté, E. Feltin, J. F. Carlin, and N. Grandjean, Phys. Rev. Lett. **98**, 126405 (2007).
[3] M. A. Baranov, M. S. Mar'enko, V. S. Rychkov, and G. V. Shlyapnikov, Phys. Rev. A **66**, 013606 (2002).
[4] T. W. Neely, E. C. Samson, A. S. Bradley, M. J. Davis, and B. P. Anderson, Phys. Rev. Lett. **104**, 160401 (2010).
[5] Z. Hadzibabic, P. Krüger, M. Cheneau, B. Battelier, and J. Dalibard, Nature (London) **441**, 1118 (2006).
[6] A. C. Potter, E. Berg, D. W. Wang, B. I. Halperin, and E. Demler, Phys. Rev. Lett. **105**, 220406 (2010).
[7] D. W. Wang, Phys. Rev. Lett. **98**, 060403 (2007).
[8] M. Kellogg, J. P. Eisenstein, L. N. Pfeiffer, and K. W. West, Phys. Rev. Lett. **93**, 036801 (2004).
[9] O. Gunawan, Y. P. Shkolnikov, E. P. DePoortere, E. Tutuc, and M. Shayegan, Phys. Rev. Lett. **93**, 246603 (2004).
[10] D. Snoke, S. Denev, Y. Liu, L. Pfeiffer, and K. West, Nature (London) **418**, 754 (2002).
[11] L. Tiemann, W. Dietsche, M. Hauser, and K. von Klitzing, New J. Phys. **10**, 045018 (2008).
[12] Y. Yoon, L. Tiemann, S. Schmult, W. Dietsche, K. von Klitzing, and W. Wegscheider, Phys. Rev. Lett. **104**, 116802 (2010).
[13] N. W. Sinclair, J. K. Wuenschell, Z. Vörös, B. Nelsen, D. W. Snoke, M. H. Szymanska, A. Chin, J. Keeling, L. N. Pfeiffer, and K. W. West, Phys. Rev. B **83**, 245304 (2011).
[14] H. K. Min, R. Bistritzer, J. J. Su, and A. H. MacDonald, Phys. Rev. B **78**, 121401 (2008).
[15] M. J. Gilbert and J. Shumway, J. Comput. Electron. **8**, 51 (2009).
[16] C. H. Zhang and Y. N. Joglekar, Phys. Rev. B **77**, 233405 (2008).
[17] M. Y. Kharitonov and K. B. Efetov, Phys. Rev. B **78**, 241401R (2008).
[18] M. Y. Kharitonov and K. B. Efetov, Semicond. Sci. Technol. **25**, 034004 (2010).
[19] S. Kim, I. Jo, J. Nah, Z. Yao, S. K. Banerjee, and E. Tutuc, Phys. Rev. B **83**, 161401 (2011).
[20] M. J. Gilbert, Phys. Rev. B **82**, 165408 (2010).
[21] E. L. Pollock and D. M. Ceperley, Phys. Rev. B **30**, 2555 (1984).
[22] D. M. Ceperley, Rev. Mod. Phys. **67**, 279 (1995).
[23] J. B. Anderson, J. Chem. Phys. **65**, 4121 (1976).
[24] D. M. Ceperley, Phys. Rev. Lett. **69**, 331 (1992).
[25] J. Shumway and D. M. Ceperley, Sol. Stat. Comm. **134**, 19 (2005).
[26] X. Zhu, P. B. Littlewood, M. S. Hybertsen, and T. M. Rice, Phys. Rev. Lett. **74**, 1633 (1995).
[27] S. DePalo, F. Rapisarda, and G. Senatore, Phys. Rev. Lett. **88**, 206401 (2002).
[28] E. L. Pollock and D. M. Ceperley, Phys. Rev. B **36**, 8343 (1987).